A Preliminary Study of Particle Velocity During Phonation in an in Vivo Canine Model

Gerald S. Berke, Dennis M. Moore, *Peter A. Monkewitz, David G. Hanson, and Bruce R. Gerratt

*Division of Head and Neck Surgery, University of California at Los Angeles School of Medicine, Los Angeles; Veteran's Administration Medical Center, West Los Angeles; and the *Department of Mechanical, Electrical and Aerospace Engineering, UCLA, Los Angeles, California, U.S.A.*

Summary: The particle velocity across the glottis was measured with simultaneous electroglottography, photoglottography, and subglottic pressure in an in vivo canine model of phonation. A constant temperature anemometer measured flow velocity at five midline anterior to posterior glottal positions. Tracheal input air flow was varied in five steps from 175 to 500 cc/s, while vocal fold approximation was achieved by constant electrical stimulation of the laryngeal nerves. For all levels of air flow, a decreasing peak velocity gradient was observed from the anterior commissure to the arytenoids. Time-varying features of the flow velocity are discussed in relation to glottal vibratory events and aerodynamics. **Key Word:** Glottal particle velocity.

This study was undertaken with the expectation that measurement of the exit glottal velocity jet from an in vivo model of phonation may help to bridge the present gap between theoretical and clinical studies of laryngeal physiology.

Synthesis of voiced sounds based on fluid mechanical vibratory models of the larynx have usually assumed one-dimensional air flow between parallel plates under quasistatic conditions (1). These assumptions neglected the influence on aerodynamics from vocal fold wall curvature and the inertial effects of the subglottic and supraglottic air columns. Recently, however, Gauffin and Liljencrants (2) have considered the resultant effect on particle velocity from convective acceleration (centrifugal force) due to wall curvature. They have shown that

$$P_c = (W/2kr_o)P \qquad (1)$$

where r_o is the radius of the curvature of the vocal folds, W the glottal width, k a constant, close to unity, P_c the pressure difference betwen the wall and the midline, and P the translaryngeal pressure drop. It thus seems that convective acceleration may cause pressure differences of the same order of magnitude as P. Furthermore, air velocity would be lowest at the midline and increase toward the surface of the folds. Thus, the true velocity profile across the glottis may vary with laryngeal geometry and may not be uniform.

Wild et al. (3) have also estimated the velocity profile along the semiminor and semimajor axes of elliptically shaped tubes containing a viscous fluid flow. The tubes' collapsed, ovoid configuration with axial narrowing has geometric similarities to the glottis. They demonstrated a higher velocity near the surface but for both semiminor and semimajor axes.

Static modeling experiments have further emphasized the importance of glottal geometry on aerodynamics. Measurements from static models have

shown significant alterations in glottal flow resistance with only minor changes in laryngeal geometry (4–7). The studies mentioned earlier indicate that the flow velocity profile may be nonuniform and, in actuality, may vary multidimensionally along the anterior to the posterior and the midline to the lateral extent of the glottis. Flanagan (8) realized the existence of this multidimensional velocity profile when he stated that in practical situations, considerable variation actually exists in the distribution of particle velocity over the orifice, and the assumption of uniform velocity distribution is not particularly good. He further comments that to determine the volume discharge at the orifice precisely it is necessary to integrate the particle velocity over the orifice area, and this requires a knowledge of the velocity profile.

Another significant factor in determining laryngeal aerodynamics may be the interaction of the subglottic and supraglottic air masses with the jet produced during rapid vocal fold oscillation. Titze (9) in his essay on the physics of small-amplitude oscillation of the vocal folds, discussed the consequence of air column inertia (momentum) on exit particle velocity. He pointed out that at fundamental frequencies below the first formant, the air column can be thought of as primarily inertive. Thus, rapid changes in vocal fold excusion may lead to supraglottal air column compression during glottal opening and rarefaction during closing. Inertially induced pressure fluctuations may consequently produce a concomitant decrease in particle velocity during glottal opening and an increase during closure.

This pressure–velocity relationship can be illustrated by analogy to the frictionless flow of a gas from a large tank through a convergent nozzle (10). By rearranging the Bernoulli equation and solving for the supraglottic (exit) velocity V_2 one obtains

$$V_2 = 1.414(P/d)^{1/2} \qquad (2)$$
$$\text{with} \quad P = P_1 - P_2 \qquad (3)$$

where V_2 is the supraglottic particle velocity or nozzle exit velocity, P the translaryngeal pressure drop or pressure drop across the nozzle, P_2 the supraglottic pressure or nozzle exit pressure, P_1 the subglottic pressure or tank pressure, and d the density of air. Thus, for a given P_1, an increase in P_2 during glottal opening (due to inertia) decreases the pressure differential (P) across the glottis, thereby de-

creasing V_2. The converse is true for a decrease in P_2 during closure.

The studies mentioned earlier on theoretical and static laryngeal models point to the necessity of studying dynamic physiologic systems. Scherer et al. (5), in discussing his static modelling experiments, commented that to obtain a more realistic approximation, it may be necessary to design oscillatory systems in which instantaneous pressures and volume flows are measured. As a preliminary step toward a more realistic appraisal of glottal flow dynamics, we studied the air velocity along the semimajor axis of the glottis in an in vivo canine preparation.

Velocity measurements were obtained in this study by using a constant temperature (hot wire) anemometer (CTA) (11,12). The hot-wire principle has been used in spirometry to measure the volume velocity wave form for both respiration and phonation. Several authors have analyzed CTA wave forms in normal subjects and in patients with laryngeal pathologic findings (13–15). Although anemometry use in aerospace engineering has been widely accepted, application to laryngeal physiology has been limited by a number of factors (16). The calibration of the instrument poses the greatest problem because the relationship of velocity to voltage output is nonlinear, and flow directionality or low velocities can be difficult to detect and interpret. In addition, the sensors are quite fragile, so that placement close to the human larynx is not feasible.

Despite these obstacles, application of CTA can potentially yield a direct measure of the volume velocity emanating from the in vivo animal larynx. Alternative techniques such as laser-Doppler velocimetry are no less problematic than anemometry. Inverse filtered pneumotachography can be used to derive volume velocity, but it is not a direct measure of velocity and provides only far-field information. Hot-film anemometer probes have been developed for use in humid environments such as the in vivo model, and there is a large body of literature dealing with calibration and flow directionality. Finally, the small size of some probes permits translation within the air stream close to the larynx without gross interference of exit flow.

This preliminary study was an attempt to obtain experimental data on the nature of the near-field glottal exit particle velocity profile and the effects of vocal fold configuration and air column inertia on

particle velocity. Further information about vocal fold movement and aerodynamics was provided by simultaneous recording of electroglottography (EGG), photoglottography (PGG), and subglottic pressure (PRS) results.

METHODS

In vivo preparation

The experimental setup was similar to prior in vivo canine studies (17,18). Dogs were anesthetized with an i.m. injection of 2 ml of Innovar followed by intravenous pentobarbital until loss of the corneal reflex was achieved. The animals were then placed supine on an operating table (Fig. 1), and direct laryngoscopy was performed to confirm normal laryngeal anatomy. A 7-mm oral endotracheal tube was inserted through which the animal breathed spontaneously. A vertical midline incision was made from the mandible to the sternum. The strap muscles and sternocleidomastoid muscles were retracted laterally to expose the larynx and trachea.
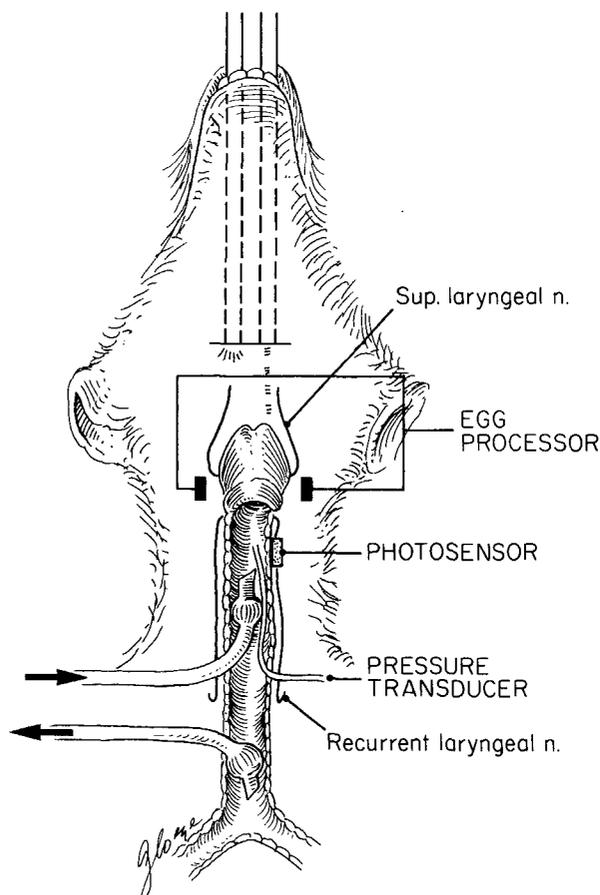

FIG. 1. Canine preparation.

The external branch of the superior laryngeal nerves were isolated at their entrance into the cricothyroid muscle. A gauze/silver electrode was applied to the nerves and insulated from the surrounding tissue. The recurrent laryngeal nerves were isolated at 5 cm inferior to the larynx, and electrodes were applied. Ground electrodes were sutured to the trachea.

Two nerve stimulators were used, one nerve stimulator (Grass model 54H) to provide voltage stimulation for the superior laryngeal nerves, while a second nerve stimulator (WPI 301-T) was used to provide a level of constant current stimulus for the recurrent laryngeal nerves. Voltages ranged from 0.5–0.6 V for the Grass stimulator. Currents ranged from 0.1–0.15 mA for the WPI stimulator. The frequency of stimulus was 80 Hz, with a pulse duration of 1.5 ms for both the Grass and WPI units. A 1-cm button was used to suspend the epiglottis anteriorly, through the thyrohyoid membrane to improve visualization of the vocal folds. A distal tracheotomy was performed, and an endotracheal tube was passed to permit the animal to breathe spontaneously. A more proximal tracheotomy was performed, through which a cuffed tracheotomy tube was placed with its tip resting 10 cm below the glottis. The catheter-tipped pressure transducer was inserted through this upper tracheotomy. The cuff of the superiorly directed tube was inflated to just seal the trachea. Tracheal air flow was passed through the cephalad tracheotomy tube.

The air was humidified and warmed by bubbling it through a 1-L pressure-sealed container filled with 100 ml of H_2O. The container was itself heated in a water bath so as to provide an air temperature in the animals' tracheas at a constant 37°C when measured at 15-min intervals.

Photoelectric and pressure measurement

The PGG light sensor (Centronics OSD 50-2) was placed on the trachea approximately 3 cm below the larynx. A xenon light source and fiberoptic cable provided supraglottic illumination for the PGG. Electroglottographic electrodes (Synchrovoice) were placed in direct contact with the thyroid cartilage while the reference electrode was sutured to the skin.

A microphone (Sennheiser) was placed 15 cm from the vocal folds and connected to a Storz model 8000 laryngostroboscope for frequency analysis of the phonatory sound. Videostroboscopic recording

after each trial was also performed using a Storz 0° laryngoscope and a Sony CCD camera (model 101) connected to a Sony recorder (VO5800).

A catheter-tipped pressure transducer (Millar, SPC 330) was calibrated at the temperature of the animals' tracheas by submerging it in a water bath at 37°C to a depth just covering the sensor (0.5 cm). The catheter was then calibrated against a manometer from 0 to 100 cm of H_2O pressure.

The PGG, EGG, PRS, and CTA voltage output signals were recorded on a four-channel Tannberg FM recorder (Model 115). The signals were also visualized on two oscilloscopes (Textronix 5116 and Hitachi V1050-F). The recorded wave forms were low-pass filtered at 1,500 Hz and digitized at a rate of 20 kHz. A 0.5-s sample of stable phonation was used for the analysis.

Data for Fig. 2 were obtained in a fourth animal by using two Millar pressure transducers model SPC 330 calibrated at 37°C from 0 to 100 cm of H_2O. One transducer was placed through the tracheostomy resting 2 cm below the glottis. The other catheter was placed through the cords from above and then withdrawn until the transducer was observed to rest 2 mm above the upper margin of the cords. The EGG, PGG, and pressure signals were recorded on a four-channel storage oscilloscope (Textronix 5116) and transferred to an XY plotter. Input tracheal air flow was set at 275 cc/s for this experiment.

Constant temperature anemometry

The fiber-film hot-wire anemometer probe was held 1 cm above the glottis by a traversing mechanism mounted at the head of the operating table.

Changes in sensor position were then precisely adjusted at 2-mm intervals along the glottal aperture.

The measurement of the unsteady air velocity downstream of the glottis was carried out by hot-wire anemometry. A DANTEC type 56C01 CTA with a DANTEC type 56C17 CTA bridge and a DANTEC type 55R01 fiber-film probe was used. The probe has an active length of 1.25 mm and is electrically insulated for use in a humid environment. The CTA probe was operated at a wire temperature of 200°C. The CTA was calibrated against a rotameter (Fig. 3), and the voltage was read on a voltmeter. The rotameter was independently calibrated against a Pitot-tube and a mercury U-tube manometer to determine the dynamic head ($1/2dU_j^2$), with d the density of moist air at 37°C (1.113×10^{-3} g/cm³) and U_j the jet velocity, (19). The rotameter (Fig. 3) was specially designed to have a 3-mm diameter opening with a converging throat to avoid air flow separation and thus provide a uniform velocity across the opening. To avoid having to correct the calibration for different ambient temperatures and especially for the unknown effect of humidity, the calibration was carried out with 100% moist air at 37°C, which corresponds to the conditions of the experiment.

The calibration curve for the CTA is shown in Fig. 4. The open circles represent the measured velocities, and the closed circles represent velocity predicted by the cubic regression

$$\text{Vel} = 441 - 419v + 125.3v^2 - 10.72v^3 \quad (4)$$

where v is the voltage output of the anemometer. The CTA was calibrated at the beginning and at the end of the experiment.
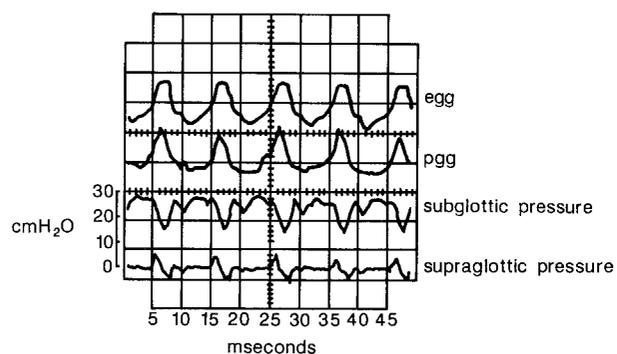
FIG. 2. Glottographic wave forms recorded for a tracheal air flow of 275 cc/s. egg, electroglottography; pgg, photoglottography; and PRS, subglottic pressure (cm of H_2O). Supraglottic pressure, cm of H_2O.
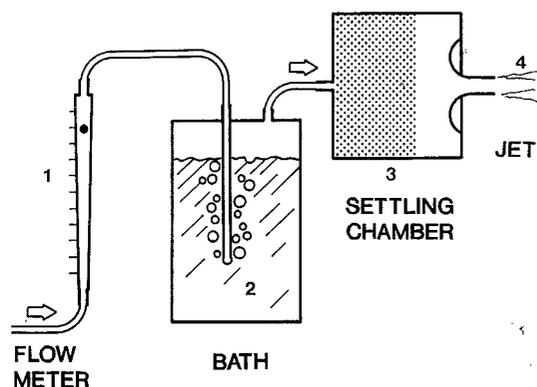
FIG. 3. Schematic of the constant temperature anemometer calibration setup with: (1) Gilmont ball-type flowmeter on compressed air supply, (2) constant temperature bath and humidifier, (3) jet settling chamber with packing of open cell foam, and (4) calibration jet of 3-mm diameter.
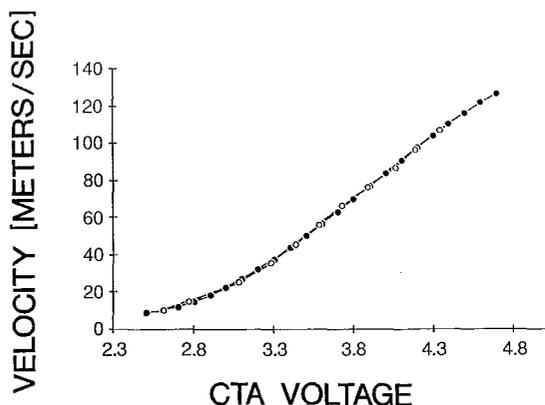
FIG. 4. Constant temperature anemometer (CTA) calibration curve: velocity Vel (meters/s) as a function of CTA voltage v (volts) (open symbols) and fitted curve defined by Eq. 4 (solid symbols).

Experimental design

Four animals were studied in the investigation. They were stimulated to phonate at 100 Hz at 275 cc/s. While holding the level of the stimulus to the recurrent and superior laryngeal nerves constant, the flow was varied, and recordings were performed for each trial. Four levels of input tracheal air flow were investigated: 175, 275, 375, and 500 cc/s. Recordings were obtained at each of the five anterior to posterior positions for each of the four input tracheal air flows (Fig. 5). Technical difficulties with CTA calibration and injury to the sensors prevented reliable results from the first two animals. The results from the third animal form the basis for this report. A fourth animal underwent PRS and supraglottic pressure measurements during phonation at 275 cc/s to study the effects of inertially induced pressure changes on particle velocity (Fig. 2).

RESULTS

Figures 6–9 display wave forms recorded for phonations near 100 Hz at tracheal air flow rates of 175, 275, 375, and 500 cc/s. The A–E designations in the figures correspond to the glottal positions schematized in Fig. 5. Table 1 enumerates the peak particle velocity for each condition. It is apparent that as input tracheal air flow was increased from 175 to 500 cc/s, measured output peak velocity increased from 69 to only 88m/s. Peak velocity most often decreased from the anterior to the posterior direction.

The rise of velocity was abrupt, and coincided with the peak of the differentiated EGG (DEGG)
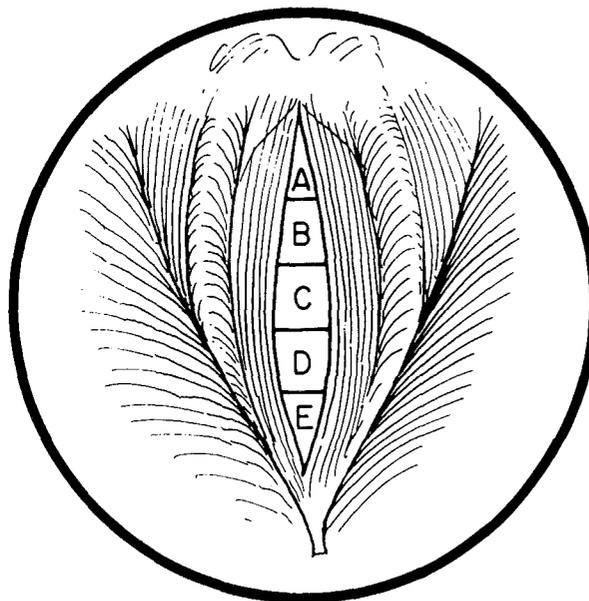

FIG. 5. Schematic diagram of canine glottis demonstrating five glottal ducts, A–E.

wave form, representing the initiation of glottal opening (Fig. 10). As the sensor was positioned more posteriorly from the anterior commissure, the abrupt rise in velocity tended to lag further behind the peak in the DEGG. There was up to about 1 ms of maximum lag at sensor position D (Fig. 11). The rise of the PGG signal before the detection of air flow by the sensor (Figs. 6–9) occurred due to light transmission from vocal fold thinning prior to horizontal opening.

The velocity wave form had a notched peak in most samples. The velocity peaked initially and then dropped acutely. As the cords began to close,
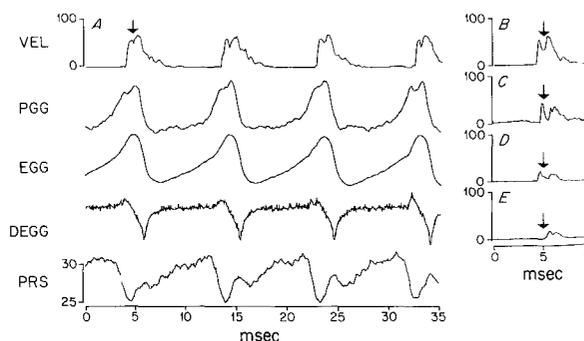

FIG. 6. Glottographic wave forms recorded for a tracheal air flow of 175 cc/s. The A–E correspond to the position of the sensor (in Fig. 5). Arrows indicate the peak of the photoglottography (PGG) for comparison of velocity profiles. VEL, velocity (m/s); EGG, electroglottography; DEGG, differentiated electroglottography; and PRS, subglottic pressure (cm of H_2O).
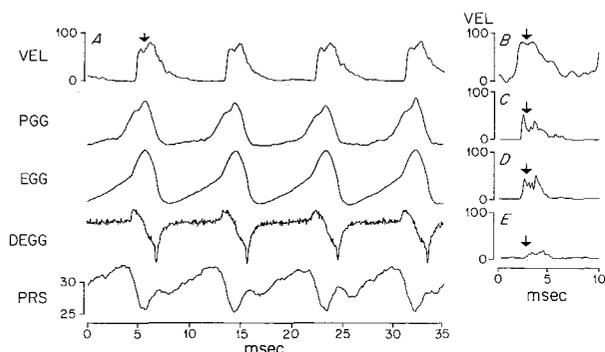
FIG. 7. Glottographic wave forms recorded for a tracheal air flow of 275 cc/s. The A–E correspond to the position of the sensor (in Fig. 5). Arrows indicate the peak of the photoglottography (PGG) for comparison of velocity profiles. VEL, velocity (m/s); EGG, electroglottography; DEGG, differentiated electroglottography; and PRS, subglottic pressure (cm of H_2O).

FIG. 9. Glottographic wave forms recorded for a tracheal air flow of 500 cc/s. The A–E correspond to the position of the sensor (in Fig. 5). Arrows indicate the peak of the photoglottography (PGG) for comparison of velocity profiles. VEL, velocity (m/s); EGG, electroglottography; DEGG, differentiated electroglottography; and PRS, subglottic pressure (cm of H_2O).

the glottal area diminished, and the velocity again rose to a second peak. A notch was observed in the velocity waveform as the velocity again increased during closure. This notch generally coincided with the peak in the PGG wave form, or maximal glottal area. Following the second peak, the velocity tapered off rapidly but less abruptly than it rose on opening. The negative deflection in the DEGG, indicating the moment of lower margin closure, coincided with the shoulder in the diminishing velocity wave form (Figs. 6–9).

Aerodynamic features of glottal activity are shown by both the PRS and the Vel wave forms. The rise of velocity is closely aligned with the fall in the PRS at vocal cord opening. At maximal opening, as denoted by the PGG peak, the PRS was close to its nadir, which corresponds to the notch in the velocity wave form. Closure of the folds' lower margins was associated with a rise in PRS.
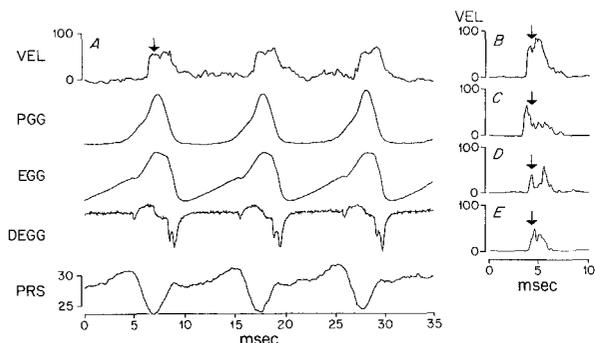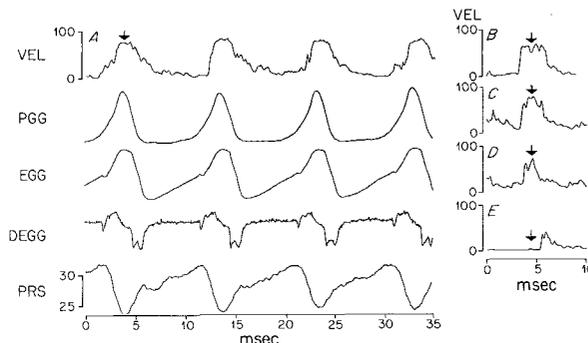
DISCUSSION

The particle velocity profile for the midline of the glottis demonstrates a decreasing gradient from the anterior commissure to the arytenoids. Whether this velocity gradient is the result of the anterior curvature of the glottis, viscous effects such as those described by Wild et al. (3), interruption of air flow by the arytenoids, or a combination of factors cannot be resolved in this study. However, one factor can be excluded. Because videostroboscopic documentation demonstrated that opening occurred from the midcord with unzipping simultaneously in both directions, the velocity gradient cannot be explained by an earlier opening time at the anterior portion of the glottis relative to the posterior portion.

A number of factors may have contributed to the lag in air flow for the posterior glottal positions (sensor positions D and E in Figs. 6–9 and 11). Inertial effects of the air column may have played a role. Figures 6–9 demonstrate that the progressive lag in the onset of air flow relative to the peak in the PGG signal correlates with the diminution in peak particle velocity from A to E. It is possible that these two phenomena are causally related. The

FIG. 8. Glottographic wave forms recorded for a tracheal air flow of 375 cc/s. The A–E correspond to the position of the sensor (in Fig. 5). Arrows indicate the peak of the photoglottography (PGG) for comparison of velocity profiles. VEL, velocity (m/s); EGG, electroglottography; DEGG, differentiated electroglottography; and PRS, subglottic pressure (cm of H_2O).

TABLE 1. *Peak particle velocity (m/s)*

Sensor position[a]	Tracheal air flow (cc/s)			
	175	275	375	500
A	69	81	75	81
B	63	81	88	69
C	38	50	75	69
D	19	38	50	56
E	19	19	50	56

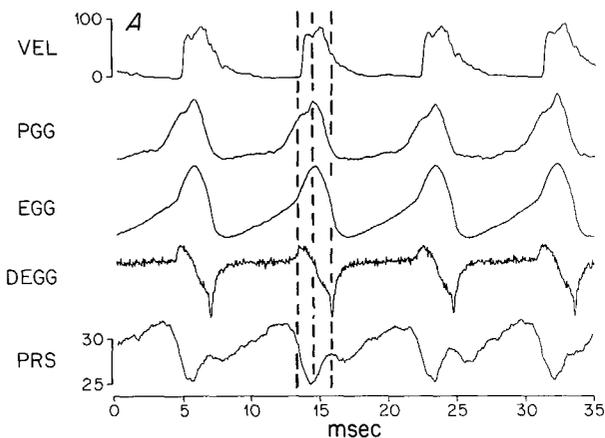[a] Positions correspond to those shown in Fig. 5.

FIG. 10. Glottographic wave forms recorded for a tracheal air flow of 275 cc/s, with the constant temperature anemometer sensor at position A (in Fig. 5). VEL, velocity (m/s); PGG, photoglottography; EGG, electroglottography; DEGG, differentiated electroglottography; and PRS, subglottic pressure (cm of H_2O). Broken lines indicate, from left to right: opening, peak opening, and closure.

lower the peak velocity attained, the longer the time for the air molecules to overcome the inertial effects of the air column and reach the sensor. Consequently, at the posterior glottis, where peak velocity is at its lowest, the time of sensor detection is the most delayed. Another factor influencing the onset time may be the vibratory nature and mass of the canine arytenoids, which required the sensor to be placed a maximum of 0.5 cm farther from the glottis for the most posterior position (E in Fig. 5) than the anterior positions (A, B, and C in Fig. 5). This 0.5-
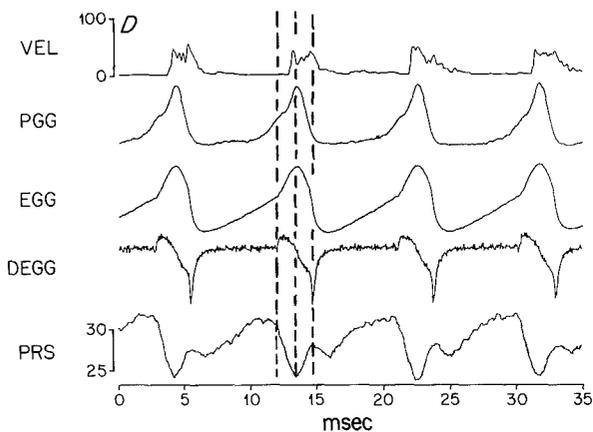

FIG. 11. Glottographic wave forms recorded for a tracheal air flow of 275 cc/s, with the constant temperature anemometer sensor at position D (in Fig. 5). VEL, velocity (m/s); PGG photoglottography; EGG, electroglottography; DEGG, differentiated electroglottography; and PRS, subglottic pressure (cm of H_2O). Broken lines indicate, from left to right: opening, peak opening, and closure.

cm displacement may have contributed to the delay in sensor detection by additional jet stream dispersion as well as the time lag due to the increased distance the particles travelled before anemometer sensing.

That peak velocity increased only modestly for increasing air flow may be a function of the mean PRS remaining relatively constant at 30 cm of H_2O. This result can be understood by examination of Eq. 2, which predicts an increase in particle velocity only when P (translaryngeal pressure) increases. Consequently, a constant PRS during increasing air flow, assuming constant vocal fold stiffness associated with constant laryngeal nerve stimulation, implies that the dynamic resistance of the system may be flow controlled. We are currently preparing a paper discussing flow-controlled nonlinear laryngeal resistance during phonation.

The notched peak of the velocity wave form provides further evidence that the inertia of the subglottic and supraglottic air columns affects glottal particle velocity. Figure 2 depicts EGG, PGG, PRS, and supraglottic pressure recordings. The translaryngeal pressure difference at the start of opening was 30 cm of H_2O. Using Eq. 2, this difference calculates to a predicted initial peak velocity of 59 m/s, a value that is close to the average measured value of 53 m/s for the input tracheal air flow of 275 cc/s presented in Table 1. Further examination of the waveforms in Fig. 2 demonstrates that as the subglottic pressure fell during opening (the rising limb of the PGG), there was a corresponding inertial rise in supraglottic pressure. These reciprocal pressure changes would have produced a net decrease in translaryngeal pressure (P). Equation 2 predicts a decrease in velocity for decreasing P. Therefore, the fall in velocity after the first velocity peak in Figs. 6–9 may have resulted from a translaryngeal pressure drop due to inertial effects. Figure 2 also depicts the supraglottic pressure returning to atmospheric at maximal opening (the peak of PGG), lowering to less than atmospheric during closure (the falling shoulder of the PGG), and at a minimum at the moment of closure (the nadir of the DEGG). During closing, inertially induced supraglottic pressure rarefaction, in conjunction with the rise in PRS, would have led to an increase of P and (using Eq. 2) to an increase in particle velocity. Thus, the second peak obtained in the velocity wave forms of Figs. 6–9 may have also been produced by air column inertia.

The tapering velocity shown in Figs. 6–9 follow-

ing the moment of glottal closure also can be explained by the inertial effects of the air column (20). Velocity dropped off abruptly at closure but then tapered off more slowly to a minimum 1–2 ms after the nadir in the DEGG. Cranen and Boves (21) have discussed this additional air flow following closure. They relate it to the escape of air flow from the posterior part of the inferior margins into the anterior space between the upper margin of the folds. Another strong possibility is that inertially induced rarefaction of the air column at glottic closure resulted in reversal of supraglottic air flow.

This investigation was an initial attempt to evaluate glottal aerodynamics in a more realistic setting than theoretical or in vitro studies. However, until a number of questions concerning the interpretation of CTA signals and the significance of turbulence and off–center-line flows are answered, extension of the results to simulated animal or human phonation should be made with caution. The goals of this study included determining the glottal velocity profile for the isolated effect of increasing tracheal air flow at constant laryngeal tension. Future investigations should strive to determine the velocity profile for various levels of glottal resistance and/or different frequencies of phonation.

SUMMARY

The technique of CTA was applied to an in vivo canine model of phonation. Particle velocity was measured for five midline anterior to posterior glottal positions. Four levels of tracheal air flow were studied. Results of this preliminary investigation lend support to the following hypotheses: A multidimensional velocity profile exists for the exit glottal jet, with a decreasing peak velocity gradient occurring from the anterior commissure to the arytenoids. The velocity of the exit glottal jet is greatly influenced by the inertia of the subglottic and supraglottic air columns, and the velocity may transiently diminish near peak opening.

REFERENCES

1. Ishizaka K, Flanagan JL. Synthesis of voiced sounds from a two-mass model of the vocal folds. *Bell System Tech J* 1972;51:1233–68.
2. Gauffin J, Liljencrants J. The role of convective acceleration in glottal aerodynamics. In: Fujimura O, ed. *Vocal fold physiology*. Vol. 2. New York: Raven Press, 1988:219–26.
3. Wild R, Pedley TJ, Riley DS. Viscous flow in collapsible tubes of slowly varying cross-section. *J Fluid Mech* 1977; 81(2):273–94.
4. Scherer R, Titze I. Pressure-flow relationships in a model of the laryngeal airway with a diverging glottis. In: Bless DM, Abbs JH, eds. *Vocal fold physiology*. San Diego: College-Hill Press, 1983:179–93.
5. Scherer RC, Titze IR, Curtis JF. Pressure-flow relationships in two models of the larynx having rectangular glottal shapes. *J Acoust Soc Am* 1983;73:668–76.
6. Gauffin J, Binh N, Ananthapadmanabha TV, Fant G. Glottal geometry and volume velocity waveform. In: Bless DM, Abbs JH, eds. *Vocal fold physiology*. San Diego: College-Hill Press, 1983:194–201.
7. Gauffin J, Binh N, Ananthapadmanabha TV, et al. Glottal geometry and glottal flow. In: *Proceedings of the vocal fold physiology conference*. Madison, WI: 1981.
8. Flanagan JL. Some properties of the glottal sound source. *J Speech Hear Res* 1958;1:99–116.
9. Titze IR. The physics of small amplitude oscillations of the vocal folds. *J Acoust Soc Am* 1988;83(4):1536–52.
10. Vennard JK. *Elementary fluid mechanics*. New York: John Wiley & Sons Inc, 1948:87–9.
11. Perry AE. *Hot-wire anemometry*. Oxford: Clarendon Press, 1982.
12. Sandborn VA. *Resistance temperature transducers*. Fort Collins, Colorado: Metrology Press, 1972.
13. Teager HM, Teager SM. The effects of separated airflow on vocalization. In: Bless DM, Abbs JH, eds. *Vocal fold physiology*. San Diego: College-Hill Press, 1983:124–43.
14. Kitajima K, Isshiki N, Tanabe M. Use of a hot-wire flow meter in the study of laryngeal function. *Studia Phonolog* 1978;112:25–30.
15. Woo P. Phonatory volume velocity recording by use of hot film anemometry and signal analysis. *Otolaryngol Head Neck Surg* 1986;95:312–8.
16. Hardy JC. Techniques of measuring intraoral air pressure and rate of airflow. *J Speech Hear Res* 1967;10:650–4.
17. Berke GS, Hantke DR, Moore DM, Hanson DG, Gerratt B. Laryngeal modeling: theoretical, in-vitro, in-vivo. *Laryngoscope* 1987;97(7):871–81.
18. Rubin HJ. Experimental studies on vocal pitch and intensity in phonation. *Laryngoscope* 1963;73:973–1015.
19. Bradshaw P. *Experimental fluid mechanics*. 1st ed. Oxford: Pergamon Press Inc, 1964:00–00.
20. Titze IR, Talkin D. Simulation and interpretation of glottographic waveforms. *ASHA Rep* 1981;11:48–55.
21. Cranen B, Boves L. On subglottal formant analysis. *J Acoust Soc Am* 1987;81(3):734–46.